




Subshell-resolved electron capture in O^{4+} -He collisions near Bohr velocity

K. Z. Lin ^{1,2}, Y. Gao,^{2,3} X. L. Zhu ^{2,3,*}, S. F. Zhang,^{2,3,†} T. Cao,^{2,3} D. L. Guo,^{2,3} X. Shan ^{1,‡},
D. M. Zhao,^{2,3} X. J. Chen,¹ and X. Ma^{2,3}

¹Department of Modern Physics, School of Physical Sciences, University of Science and Technology of China, Hefei 230026, China

²Institute of Modern Physics, Chinese Academy of Sciences, Lanzhou 730000, China

³University of Chinese Academy of Sciences, Beijing 100049, China



(Received 6 February 2024; accepted 17 April 2024; published 9 May 2024)

Subshell-resolved single-electron capture has been investigated in collisions between O^{4+} ions and He atoms at energies from 7 to 70 keV/nucleon, using high-resolution cold-target recoil-ion momentum spectroscopy. Analysis of the Q -value spectra, n -shell dependence, relative branching ratios, and angular distributions provides insight into the dominant reaction channels. Capture into the $n = 3$ state remains dominant in the entire projectile energy, agreeing with predictions from the molecular Coulombic over barrier model. At low energies, capture preferentially populates the $3s$ subshell, while higher l states like $3d$ become dominant at higher projectile energies. The oscillatory transverse momentum distribution of $3s$ states is attributed to de Broglie wave Fraunhofer diffraction, indicative of the quantum nature of the collision dynamics.

DOI: [10.1103/PhysRevA.109.052811](https://doi.org/10.1103/PhysRevA.109.052811)

I. INTRODUCTION

Electron capture processes, which involve the capture of one or several target electrons by an energetic ion during collisions with neutral atoms, are considered to be among the most fundamental charge-changing interactions. Due to their significant role in both fundamental and applied research, electron capture processes have garnered considerable attention. From a fundamental perspective, the study of electron capture processes is crucial for understanding quantum few-body and many-body problems, such as electron-electron correlation and strong Coulombic interactions. These processes provide valuable insights into atomic structure [1,2]. Apart from their fundamental importance, electron capture processes also play pivotal roles in various applied fields, such as astrophysics [3,4] and fusion plasma physics [5,6]. As accurate collision cross sections are crucial for interpreting phenomena in these fields, extensive research efforts have been devoted to understanding electron capture processes [7–10].

From a theoretical perspective, the simple classical overbarrier model (OBM) provides reasonable predictions on capture cross sections for the principle quantum number n [11,12]. Mann *et al.* [13] suggested that double-electron capture in the collision of slow O^{6+} and C^{4+} ions with rare gas atoms occurs through one-step capture, based on the OBM model. Niehaus *et al.* [14] proposed the molecular Coulombic overbarrier model (MCBM), i.e., the reaction window theory, taking into account some influence of the projectile velocity, and the predicted widths of energy gain spectra were in agreement with the experimental results for Ar^{6+} -Ar collisions at

500 eV (velocity $v_0 = 0.022$ a.u.) and C^{4+} -He collisions at 40 keV ($v_0 = 0.365$ a.u.).

In addition to the classical OBM method and MCBM method, the atomic-orbital close-coupling (AOCC) and molecular-orbital close-coupling (MOCC) approaches have been shown to have advantages in the intermediate energy range [15–20]. The semiclassical atomic-orbital close-coupling (SCAOCC) approach provides good agreement between theoretical calculations and experimental results for the collision of C^{4+} ions with He atoms [21,22]. The classical trajectory Monte Carlo (CTMC) method has also been used to provide a reasonable description in the intermediate energy range [23–29].

However, current theoretical approaches still face challenges in the intermediate projectile energy range and multielectron systems due to the strong coupling of various reaction channels. Therefore, classical models remain important theoretical methods for investigating ion-atom collisions.

From an experimental perspective, most experiments in the past decades have focused on the energy dependence of total absolute cross sections and emission spectra in ion collision [30,31]. However, there have been relatively few studies on differential cross sections, which provide more information about collision dynamics. [32–38]. Among these studies, Gao *et al.* [38] measured the angular distributions for electron capture in He^+ -He collision, which observed pronounced oscillations. They stated that the oscillation patterns arise as a consequence of the interference between the gerade and ungerade scattering amplitudes, classical trajectory-dependent effects, and the diffraction of the matter wave of the projectile by the target.

The development of cold-target recoil-ion-momentum spectroscopy (COLTRIMS) [10,39] has provided a powerful method to measure state-selective cross sections and angular-differential cross sections due to its unique ability in

*zhuxiaolong@impcas.ac.cn

†zhangshf@impcas.ac.cn

‡xshan@ustc.edu.cn

coincidence measurement on the recoil ions with scattering projectile. Guo *et al.* employed COLTRIMS to obtain n shells state-selective cross sections and angular-differential cross sections in collisions involving protons and He^+ ions with He atoms at intermediate projectile energies [40,41]. The results exhibited favorable agreement with theoretical calculations. Abdalla *et al.* [42] and Zhang *et al.* [43,44] studied the electron capture process in the collision of Ar^{8+} ions with He atoms, and distinguished electron capture into $4s$, $4p$, and $4d$ and $4f$ subshell states, along with $3p$ and $3d$ states. Zhang *et al.* [44] verified the importance of electronic correlations by comparing experimental angular distributions with the AOCC calculations. Additionally, relative state-selective cross sections of subshells $3s$ and $3p$ and $3d$ were reported in the collision of C^{5+} ions with He atoms [45,46]. Furthermore, all subshells degenerated to $n = 3$ and $n = 4$ were delineated only in the collision of Ne^{7+} ions with He atoms [2]. However, investigations on electron capture into subshell state-selective cross sections and angular-differential cross sections remain limited. It is evident that more experiments on subshell-resolved cross sections are imperative.

In this work, we present experimental findings from the collision of O^{4+} ions with He atoms at projectile energies ranging from 7 to 70 keV/nucleon. Using the longitudinal COLTRIMS technique, we were able to determine the relative state-selective cross sections and transverse momentum distributions of the collision with subshell resolution at intermediate projectile energies. Our results revealed that the dominant channel is the electron captured into the $n = 3$ state, which is in excellent agreement with the reaction window calculated using the MCBM method. Additionally, we obtained the relative branching ratio for different nl shells as a function of projectile energy. Furthermore, we examined the transverse momentum distributions for different l population within the $n = 3$ shell. The observed oscillation structure can be attributed to Fraunhofer-type diffraction of the O^{4+} projectile de Broglie wave, which arises due to the limited spatial region for single electron capture.

II. EXPERIMENTAL SETUP

In the experiment, O^{4+} ions generated in a 14.5-GHz electron cyclotron resonance (ECR) ion source are extracted, charge-selected and accelerated to the desired energy before entering the collision chamber of the COLTRIMS system. The time of flight (TOF) system consists of a 380-mm-long path, with the angle between the TOF axis and the projectile beam measuring approximately 14° (see details in Ref. [47]). The primary O^{4+} ion beam is separated from the O^{3+} scattered projectile using an electrostatic deflector and a dipole magnet located downstream from the collision chamber. The uncollided O^{4+} ions are collected by a Faraday cup, while the O^{3+} ions are detected by another position-sensitive detector. An electrostatic field of 0.81 V/cm is employed to extract the recoil ions. The recoil ion He^+ is measured in coincidence with the scattered projectile O^{3+} . The longitudinal momentum resolution of the system is estimated to be approximately 0.08 a.u. in the z direction (projectile beam direction) and the transverse momentum resolution is about 0.28 a.u. perpendicular to the beam direction. In our studies, capture processes

with projectile energies of 7, 9, 11.5, 16.67, 25, 35, 50, and 70 keV/nucleon are investigated.

III. RESULTS AND DISCUSSION

By considering energy and momentum conservation in a single electron capture reaction, we can determine the longitudinal momentum transferred to the recoil ion using the equation

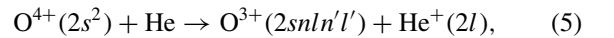
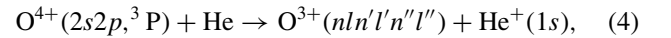
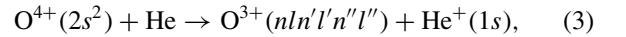
$$P_z = -\frac{Q}{v_p} - \frac{v_p}{2}. \quad (1)$$

Here, Q represents the difference between the total internal energies of the projectile and the target, while v_p denotes the projectile velocity. The longitudinal momentum distributions provide insights into the states of the projectile products. While the transverse momentum P_t of the recoil ion is linked to the scattering angle θ of the projectile through the equation

$$P_t = \theta P_0. \quad (2)$$

In this equation, P_0 represents the projectile initial momentum. This relationship allows us to analyze the differential cross sections and gain a deeper understanding of the dynamics of the populated states.

The two-dimensional spectrum in Fig. 1 displays the longitudinal and transverse recoil ion momentum, specifically for the projectile energy of 7 keV/nucleon. The spectrum projected on the horizontal and vertical axes corresponds to the longitudinal and transverse momentum, respectively, representing partial cross sections and projectile scattering angle. The captured channels shown in Fig. 1 are as follows:



which are marked by black, red, and blue text, respectively.

Figure 1 illustrates that at the given projectile energy, the primary capture event predominantly occurs within the $n = 3$ shell of O^{3+} ($3l$), with distinct subshell channels being evident. There is also observable, albeit weaker, capture into the $n = 2$ shell [$\text{O}^{3+}(2p)$] and $n = 4$ shell [$\text{O}^{3+}(4l)$]. The occurrence of the metastable state $\text{O}^{4+}(2s2p\ ^3P)$ in the projectile is remarkably low, leading to its negligible contribution to the overall capture process. In addition to the primary single-capture events, Fig. 1 also reveals secondary processes such as transfer target excitation (TTE), characterized by single capture into the $2p$ state of O^{3+} coupled with the excitation of He^+ into the $n = 2$ states, and concurrent single capture alongside projectile-core excitation (PCE), i.e., single capture into $2p$ coupled with the excitation of $2s$ of $\text{O}^{4+}(2s^2)$ into the $2p$ state [$\text{O}^{3+}(2s2p^2, 2p^3)$]. Furthermore, the transverse momentum associated with reactions involving capture into the $n = 4$ shell is consistently higher than that for capture into the $n = 3$ shell. This trend aligns with the observation in C^{5+} ion interactions with helium [45,46], where the energy curve for $n = 3$ state may cross the entrance channel while for $n = 4$ state it does not at large impact parameters [45].

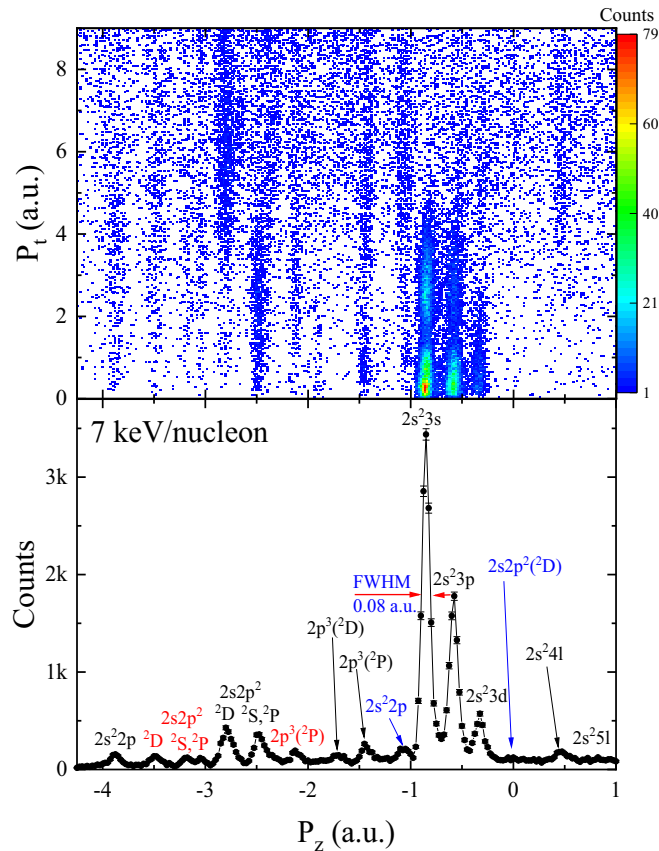


FIG. 1. Two-dimensional momentum and longitudinal distributions for single-electron capture in $O^{4+} + He$ collisions at a projectile energy of 7 keV/nucleon. The black, red, and blue text indicates capture into the ground state O^{4+} ($2s^2$), capture into the metastable state O^{4+} ($2s2p\ ^3P$), and capture into the ground state with transfer excitation processes, respectively.

Consequently, electron capture into the $n = 4$ state may be more likely to occur at small impact parameters, i.e., higher transverse momentum.

A. State-selective electron capture cross sections

Figure 2 illustrates the Q -value spectra and the reaction-window results from molecular Coulombic over barrier model (MCBM) across varying projectile energies, with the theoretical outcomes being standardized to the experimental peak values. The blue vertical lines in the figure delineate the Q -value corresponding to electron capture into discrete states, and the values at the intersections of these lines with the reaction windows demarcate the state-selective cross sections as predicted by MCBM. It is observed that electron capture into the $n = 3$ shell remains the dominant process, as evidenced in Fig. 2; this dominance persists with increasing projectile energy. It is worth noting that the data for different energies exhibit similar characteristics. Simultaneously, the propensity for electron capture into the $n = 2$ shell, as well as into higher shells such as $n = 4$, exhibits a gradual rise, additionally, the channel of $n \geq 5$ is opened with projectile energy increase and becomes significant at higher projectile energy. This trend aligns well with MCBM's theoretical projections,

which attribute the increase to an expansion of the reaction window. In contrast, the relative cross sections for PCE of the ground state and metastable state O^{4+} and TTE processes demonstrate a decline with increasing projectile energies, becoming marginally significant at 50 and 70 keV/nucleon. The PCE and TTE involve multielectron processes, necessitating more time for the adjustment of electron distribution to adapt to the changing potential. However, as the velocity of the projectile increases, the interaction time diminishes. Consequently, the cross sections of both processes may decrease. While the channel of capture into $2s$ for the metastable state O^{4+} is opened with the projectile energy increase, which is agreement with the ground state O^{4+} that the contribution of capture into ground state $2p$ exhibits a rise with increasing projectile energy. Notably, experimental data at a lower projectile energy of 7 keV/nucleon indicate that within the $n = 3$ subshell channels (the most prominent for electron capture) capture into the $3s$ state is dominant. As the projectile energy increases, the contribution from higher angular momentum states (l) grows, culminating in the $3d$ state's dominance at higher projectile energies. This experimental finding is at odds with MCBM predictions which underestimates the $3d$ yield and overestimates the $3s$ and $3p$ yields for 25–70 keV/nucleon collision energies and posits sustained dominance of the $3s$ state across the entire range of tested energies.

Figure 3 delineates the branching ratios of electron capture into the n shell and subshell as a function of the projectile energies, with Figs. 3(a) and 3(b) representing each, respectively. It is imperative to note that the presented theoretical results are predicated solely on the scenario of pure single capture. Meanwhile, the experimental branching ratios have been derived from Gaussian fits to the Q -value spectra.

As discerned from Fig. 3(a), electron capture into the $n = 3$ shell emerges as the preminent reaction pathway across the entire energy spectrum, according to our experimental observations. With an increase in projectile energy, the branching ratio for $n = 3$ capture exhibits a decline. Conversely, the branching ratios for capture into other n shells exhibit an increase. Comparatively evaluating experimental data for n shell resolutions against theoretical predictions in Fig. 3(a), the trend of relative branching ratio with the projectile energy predicted by MCBM aligns with experimental results. In addition, the magnitudes of cross sections for $n = 3$ and $n = 4$, as predicted by MCBM, correspond with experimental results within the projectile energy range of 7–11.5 keV/nucleon. Whereas discrepancies emerge between experimental and theoretical results as projectile energy increases. The cross sections for other n states show a disagreement between experimental and theoretical results.

Figure 3(b) addresses the subshell dynamics, where at lower projectile energies, the $3s$ state of O^{3+} is identified as the primary capture channel. The branching ratio for this state diminishes as projectile energy increases, while the opposite trend is observed for capture into the $3d$ state, which becomes increasingly dominant at higher energies. The $3p$ state's branching ratio initially rises with projectile energy but subsequently declines. Generally, with increased collision velocity, there is a propensity for electron capture into higher l states, an observation supported by the works of

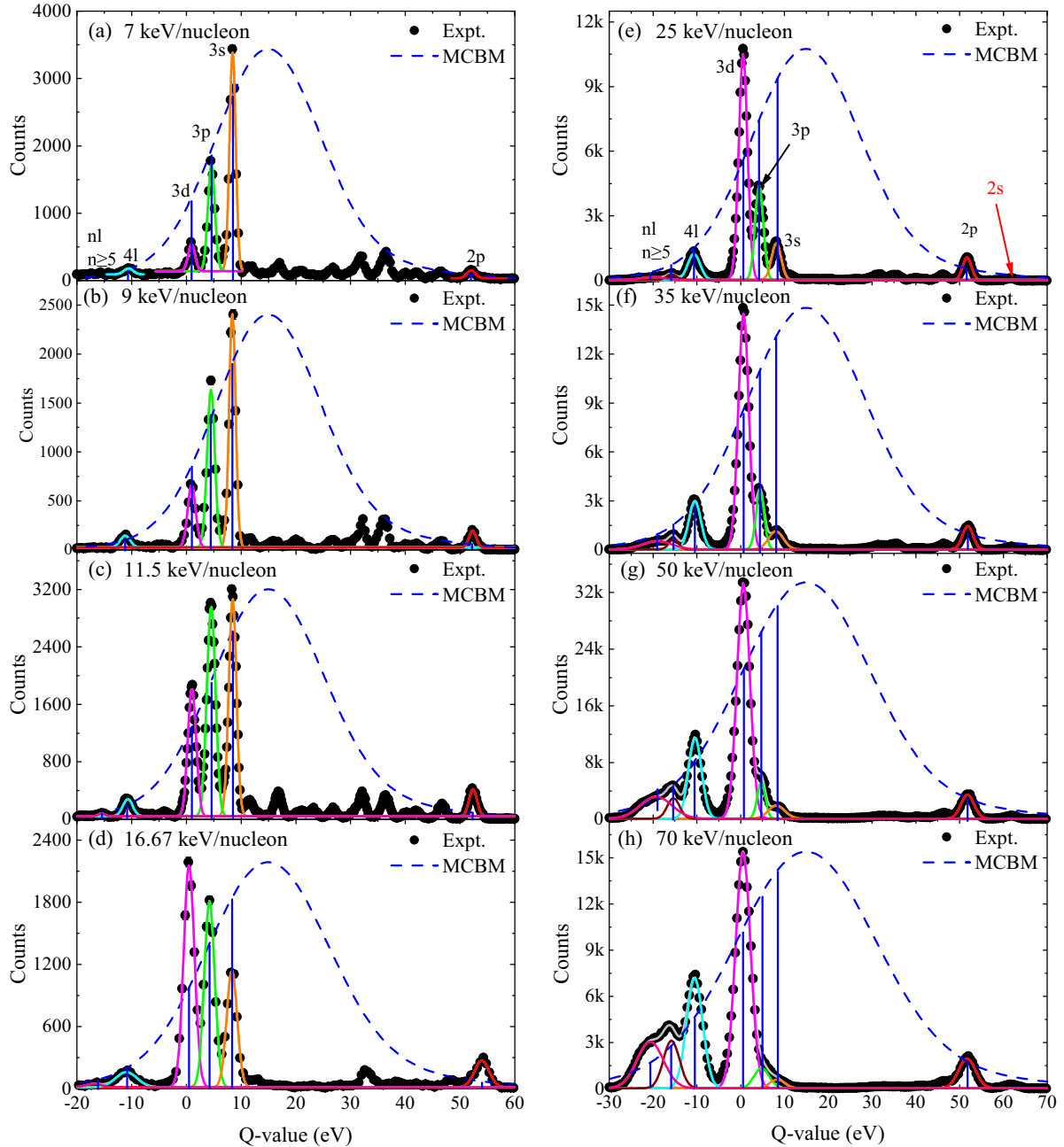


FIG. 2. Q -value spectra for single electron capture in $O^{4+} + He$ collisions at varying projectile energies. The dots denote the experimental data, while the blue dashed curves illustrate the reaction windows calculated using the MCBM method. The curves in various colors result from multi-peak Gaussian fits with fixed peak positions. The vertical lines indicate the Q -values for electron capture into distinct n states.

Abdallah *et al.* [42] and Kamber *et al.* [46] in their studies of single-electron capture by Ar^{8+} and C^{5+} ions from helium, respectively. These findings can be attributed to the conservation of angular momentum; in the projectile's rest frame, the classical angular momentum of a target electron is approximately bv_p (~ 2.25 a.u. at $v_p = 1$ a.u.), where b represents the classical barrier radius. This angular momentum is substantial enough to favor the population of states with higher angular momentum projections perpendicular to the collision plane as energy increases, thus enhancing the likelihood of capture into higher l states at increased projectile energies.

B. Transverse momentum distributions

Figure 4 illustrates the transverse momentum distributions observed for the $3s$, $3p$, and $3d$ channels at projectile energies of 7, 9, 11, 16.67, 25, 35, and 50 keV/nucleon. It should be noted that the distribution for a projectile energy of 70 keV/nucleon is not included due to the resolution constraints. The transverse momentum distributions for the $3s$ channels feature a prominent peak and a shoulder structure at small transverse momentum marked by black arrows. Additionally, the data reveal an oscillatory pattern at larger transverse momentum, characterized by double peaks in the $3s$

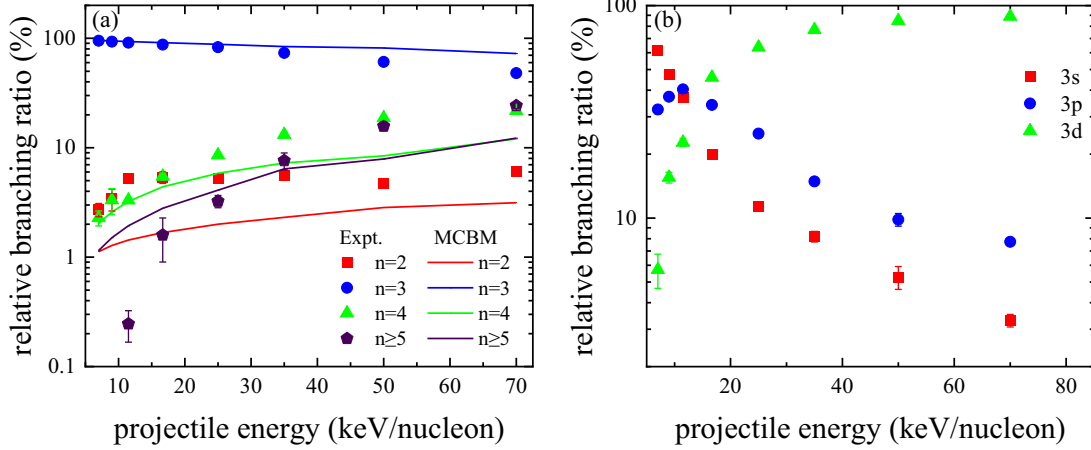


FIG. 3. Relative branching ratios plotted as a function of projectile energy for single electron capture in $O^{4+} + He$ collisions, with (a) resolution by n shells and (b) subshell resolution for the $n = 3$ state. The data points (dots) correspond to experimental measurements, while the solid lines depict the results obtained from the MCBM.

channels at lower projectile energies. This pattern becomes less pronounced at higher energies as the transverse momentum declines with the projectile energy increasing.

The oscillatory nature of the electron capture from the s state into the s state, consistent with a Fraunhofer-type diffraction, was observed in earlier studies [38,41,48–52]. This phenomenon occurs because electron capture is limited to the spatial region proximal to the target. As the projectile traverses this region, it behaves analogously to a matter wave with a wavelength λ , given by $\lambda = 2\pi/P_0$. Consequently, the scattering angular distribution exhibits alternating minima and maxima akin to an optical diffraction pattern which can be described as

$$\theta_{\min/\max} = \text{const.} \times 2\pi/(\rho P_0), \quad (6)$$

where ρ is the radius of the effective circular aperture. Associating Eq. (2) with Eq. (6), the first and second minima (dark fringes) and maxima (bright fringes) are theoretically located at

$$P_{t \text{ 1st,min}} = 0.61 \frac{2\pi}{\rho}, \quad (7)$$

$$P_{t \text{ 1st,max}} = 0.819 \frac{2\pi}{\rho}, \quad (8)$$

$$P_{t \text{ 2nd,min}} = 1.116 \frac{2\pi}{\rho}. \quad (9)$$

The position of the first dark fringe is determined from the experimental transverse momentum distributions and marked with blue dashed line and word $P_{t \text{ 1st,min}}$ in Fig. 4. Notably, the positions of the minima are roughly invariable for different projectile energies, suggesting that the aperture radius may be independent of projectile energy. The aperture radius is estimated to be about 2.25 a.u., according to Eq. (7) and the observed positions (1.7 a.u.) of the minima. Previous studies have also indicated that the maximum of the impact parameter, i.e., ρ , is also roughly independent of projectile energy [22,41,44]. Using the deduced aperture radius ρ , we can infer that the theoretical positions of the first bright fringes, which

are indicated by red dashed line. The correlation between the positions of the red dashed line and the experimental maxima at large scattering angles corroborates the interpretation that the oscillatory structures in the $3s$ state angular distributions stem from Fraunhofer-type diffraction. Additionally, the deduced position of the second dark fringe is also marked in Fig. 4, however, the predicted minimum is not observed. Previous studies illustrated the “way in” and “way out” capture pathways in the two-state picture of trajectories [53,54]. The overlap of two pathways could make the minima obscure, and it may also result in the shoulder structure at small transverse momentum.

The transverse momentum distributions for the $3p$ state also exhibit a shoulder structure and oscillatory pattern in lower projectile energies. For the $3d$ state, the oscillatory pattern is obscure, and only a broad peak appears at small transverse momentum. The oscillations for the $3p$ state, similar to $3s$ state, may be also attributed to the Fraunhofer-type diffraction. The previous study revealed that the diffraction appears in electron capture for $\Delta m_l = 0$ [22]. In the present case, a similar process maybe occur for the $3p$ state, in which electron capture into the $3p$ state tends to occupy the orbit of $m_l = 0$.

IV. CONCLUSION

In summary, we conducted a thorough investigation of single-electron capture in O^{4+} and helium collisions over an intermediate projectile energy range between 7 keV/nucleon and 70 keV/nucleon. Employing high-resolution longitudinal cold target recoil ion momentum spectroscopy (COLTRIMS), we successfully acquired high-resolution Q -value spectra. This technique facilitated the extraction of the relative branching ratios with distinct resolution for individual n shells, specifically for the pure single capture process, and for subshell resolution within the $n = 3$ channel.

Our findings reveal that, at the level of n shells resolution, the capture into the $n = 3$ state consistently represents the predominant channel throughout the entire range of projectile energies examined. However, as the projectile energy increases, the prevalence of the $n = 3$ channel diminishes in

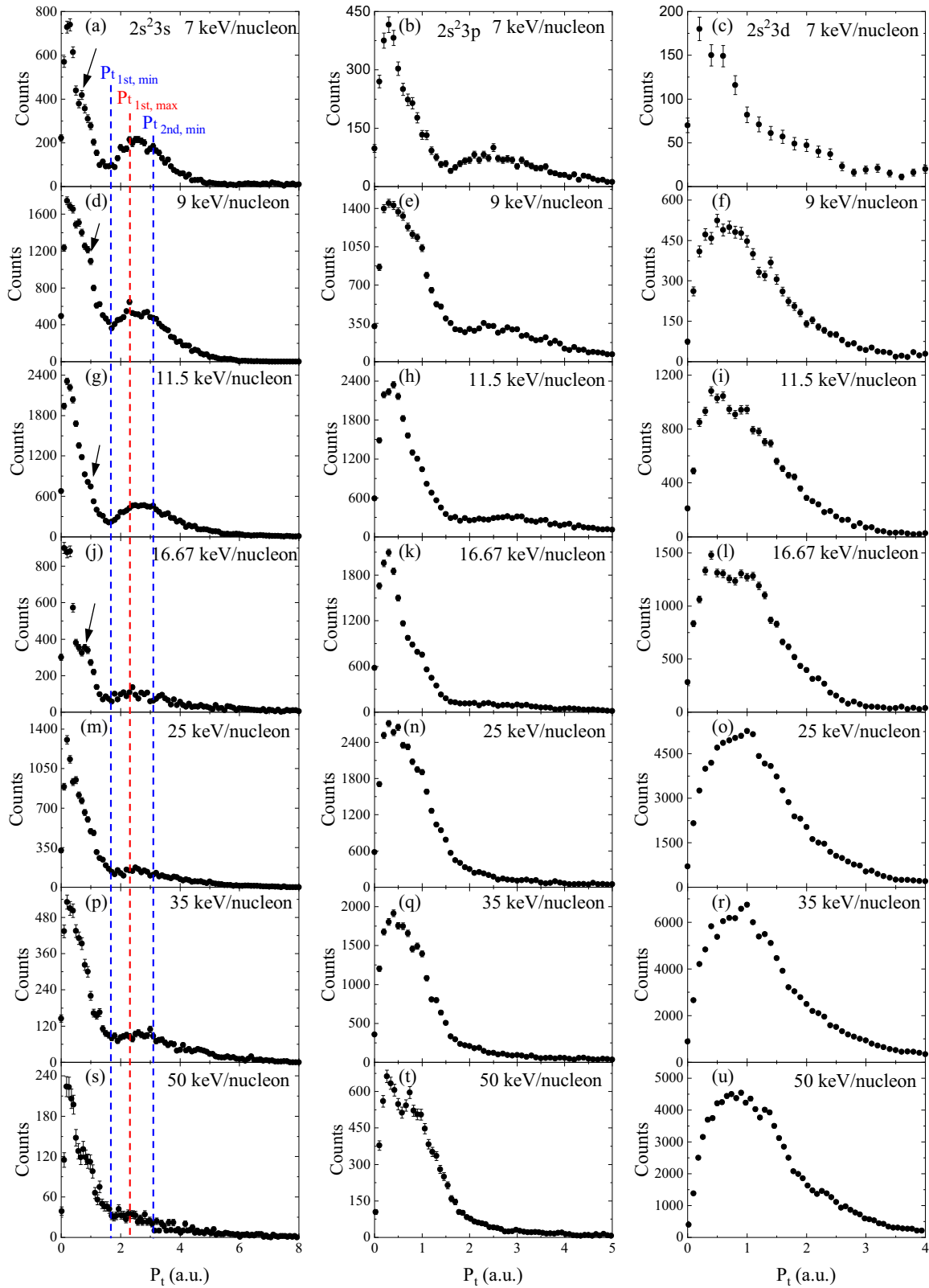


FIG. 4. Experimental transverse momentum distributions for electron capture into the $3s$, $3p$, and $3d$ states at various projectile energies. The blue dashed line indicates the position of the dark fringe in the Fraunhofer-type diffraction pattern. The red dashed line marks the position of the first bright fringe, which is inferred from the location of the first dark fringe in the Fraunhofer diffraction pattern.

favor of other n shell channels. At the subshell resolution, the $3s$ orbital capture emerges as the primary channel at lower projectile energies, which shifts with an increase in projectile energy, where higher l subshells gain significance driven by the conservation of angular momentum, making the $3d$ subshell the most prominent reaction channel. Also, we obtained the transverse momentum distributions for the $3s$, $3p$, and $3d$ subshells. The observed oscillatory pattern in the $3s$ distribution is interpreted as a matter-wave phenomenon analogous to Fraunhofer-type diffraction.

Moreover, we applied the molecular classical over barrier model to compute both the reaction window and the theoretical relative branching ratios and found that the classical theory only can qualitatively forecast the cross sections as a function of projectile energy. Thus, more accurate semiclassical or full quantum-mechanical theory is needed for quantitative predictions of cross sections and analysis of dynamics process. The precise subshell resolved relative state-selective cross

sections and differential cross sections obtained in the present experiment provide experimental benchmarks available for the development of multielectrons semiclassical or quantum calculation.

ACKNOWLEDGMENTS

This work was supported by the National Key Research and Development Program of China (Grant No. 2022YFA1602500), the National Natural Science Foundation of China (Grants No. 11974358 and No. 11934004), and the Strategic Key Research Program of the Chinese Academy of Sciences (Grant No. XDB34020000). We also thank the engineers of the 320 kV platform for providing us with the high-quality ion beam and for their assistance during the experiment. Y. Gao acknowledges the support from Young Scholars in Western China of Chinese Academy of Sciences.

-
- [1] H. Gegier, E. Marsden, and E. Rutherford, *Proc. R. Soc. London. Ser. A* **82**, 495 (1909).
- [2] D. Fischer, B. Feuerstein, R. D. DuBois, R. Moshhammer, J. R. C. López-Urrutia, I. Draganic, H. Lörch, A. N. Perumal, and J. Ullrich, *J. Phys. B: At. Mol. Opt. Phys.* **35**, 1369 (2002).
- [3] T. E. Cravens, *Science* **296**, 1042 (2002).
- [4] P. Beiersdorfer, K. R. Boyce, G. V. Brown, H. Chen, S. M. Kahn, R. L. Kelley, M. May, R. E. Olson, F. S. Porter, C. K. Stahle, and W. A. Tillotson, *Science* **300**, 1558 (2003).
- [5] R. C. Isler, *Phys. Scr.* **35**, 650 (1987).
- [6] R. C. Isler, *Plasma Phys. Control. Fusion* **36**, 171 (1994).
- [7] D. R. Bates and J. T. Lewis, *Proc. Phys. Soc. A* **68**, 173 (1955).
- [8] B. Zygelman and A. Dalgarno, *Phys. Rev. A* **33**, 3853 (1986).
- [9] P. Roncin, M. N. Gaboriaud, M. Barat, and H. Laurent, *Europhys. Lett.* **3**, 53 (1987).
- [10] R. Dörner, V. Mergel, O. Jagutzki, L. Spielberger, J. Ullrich, R. Moshhammer, and H. Schmidt-Böcking, *Phys. Rep.* **330**, 95 (2000).
- [11] H. Ryufuku, K. Sasaki, and T. Watanabe, *Phys. Rev. A* **21**, 745 (1980).
- [12] R. Mann, F. Folkmann, and H. F. Beyer, *J. Phys. B: At. Mol. Phys.* **14**, 1161 (1981).
- [13] R. Mann and H. Schulte, *Z. Phys. D* **4**, 343 (1987).
- [14] A. Niehaus, *J. Phys. B: At. Mol. Phys.* **19**, 2925 (1986).
- [15] W. Fritsch and C. D. Lin, *Phys. Rep.* **202**, 1 (1991).
- [16] W. Fritsch and C. D. Lin, *Phys. Rev. A* **54**, 4931 (1996).
- [17] J. P. Hansen, A. Dubois, and S. E. Nielsen, *Phys. Rev. A* **45**, 184 (1992).
- [18] R. J. Allan, C. Courbin, P. Salas, and P. Wahnon, *J. Phys. B: At. Mol. Opt. Phys.* **23**, L461 (1990).
- [19] N. Toshima, *Phys. Rev. A* **59**, 1981 (1999).
- [20] T. G. Winter, *Phys. Rev. A* **87**, 032704 (2013).
- [21] J. W. Gao, Y. Wu, N. Sisourat, J. G. Wang, and A. Dubois, *Phys. Rev. A* **96**, 052703 (2017).
- [22] D. L. Guo, J. W. Gao, S. F. Zhang, X. L. Zhu, Y. Gao, D. M. Zhao, R. T. Zhang, Y. Wu, J. G. Wang, A. Dubois, and X. Ma, *Phys. Rev. A* **103**, 032827 (2021).
- [23] R. Dörner, V. Mergel, R. Ali, U. Buck, C. L. Cocke, K. Froschauer, O. Jagutzki, S. Lencinas, W. E. Meyerhof, S. Nüttgens, R. E. Olson, H. Schmidt-Böcking, L. Spielberger, K. Tökesi, J. Ullrich, M. Unverzagt, and W. Wu, *Phys. Rev. Lett.* **72**, 3166 (1994).
- [24] A. Cassimi, S. Duponchel, X. Flechard, P. Jardin, P. Sortais, D. Hennecart, and R. E. Olson, *Phys. Rev. Lett.* **76**, 3679 (1996).
- [25] R. Dörner, H. Khemliche, M. H. Prior, C. L. Cocke, J. A. Gary, R. E. Olson, V. Mergel, J. Ullrich, and H. Schmidt-Böcking, *Phys. Rev. Lett.* **77**, 4520 (1996).
- [26] R. Moshhammer, J. Ullrich, H. Kollmus, W. Schmitt, M. Unverzagt, O. Jagutzki, V. Mergel, H. Schmidt-Böcking, R. Mann, C. J. Wood, and R. E. Olson, *Phys. Rev. Lett.* **77**, 1242 (1996).
- [27] V. Mergel, R. Dörner, M. Achler, K. Khayyat, S. Lencinas, J. Euler, O. Jagutzki, S. Nüttgens, M. Unverzagt, L. Spielberger, W. Wu, R. Ali, J. Ullrich, H. Cederquist, A. Salin, C. J. Wood, R. E. Olson, D. C. V. Belkić, C. L. Cocke, and H. Schmidt-Böcking, *Phys. Rev. Lett.* **79**, 387 (1997).
- [28] H. Kollmus, R. Moshhammer, R. E. Olson, S. Hagmann, M. Schulz, and J. Ullrich, *Phys. Rev. Lett.* **88**, 103202 (2002).
- [29] R. E. Olson, T. J. Gay, H. G. Berry, E. B. Hale, and V. D. Irby, *Phys. Rev. Lett.* **59**, 36 (1987).
- [30] M. B. Shah and H. B. Gilbody, *J. Phys. B: At. Mol. Phys.* **14**, 2361 (1981).
- [31] S. Bliman, A. Barany, M. Bonnefoy, J. J. Bonnet, M. Chassevent, A. G. Fleury, D. Hitz, E. J. Knystautas, J. Nordgren, J. E. Rubensson, and M. G. Suraud, *J. Phys. B: At. Mol. Opt. Phys.* **25**, 2065 (1992).
- [32] R. D. DuBois, *Phys. Rev. A* **39**, 4440 (1989).
- [33] M. B. Shah and H. B. Gilbody, *J. Phys. B: At. Mol. Phys.* **18**, 899 (1985).
- [34] M. B. Shah, P. McCallion, and H. B. Gilbody, *J. Phys. B: At. Mol. Opt. Phys.* **22**, 3037 (1989).
- [35] A. Kivimäki, A. Naves de Brito, S. Aksela, H. Aksela, O.-P. Sairanen, A. Ausmees, S. J. Osborne, L. B. Dantas, and S. Svensson, *Phys. Rev. Lett.* **71**, 4307 (1993).

- [36] T. Hayakawa, R. A. Lomsadze, C. Verzani, H. Watanabe, H. Tanuma, B. D. DePaola, and N. Kobayashi, *Phys. Scr.* **2001**, 322 (2001).
- [37] S. Bliman, R. Bruch, M. Cornille, A. Langereis, and J. Nordgren, *Phys. Rev. A* **66**, 052707 (2002).
- [38] R. S. Gao, L. K. Johnson, D. A. Schafer, J. H. Newman, K. A. Smith, and R. F. Stebbings, *Phys. Rev. A* **38**, 2789 (1988).
- [39] J. Ullrich, R. Moshhammer, A. Dorn, R. Dörner, L. P. H. Schmidt, and H. Schmidt-Böcking, *Rep. Prog. Phys.* **66**, 1463 (2003).
- [40] D. L. Guo, X. Ma, S. F. Zhang, X. L. Zhu, W. T. Feng, R. T. Zhang, B. Li, H. P. Liu, S. C. Yan, P. J. Zhang, and Q. Wang, *Phys. Rev. A* **86**, 052707 (2012).
- [41] D. L. Guo, X. Ma, R. T. Zhang, S. F. Zhang, X. L. Zhu, W. T. Feng, Y. Gao, B. Hai, M. Zhang, H. B. Wang, and Z. K. Huang, *Phys. Rev. A* **95**, 012707 (2017).
- [42] M. A. Abdallah, W. Wolff, H. E. Wolf, E. Sidky, E. Y. Kamber, M. Stöckli, C. D. Lin, and C. L. Cocke, *Phys. Rev. A* **57**, 4373 (1998).
- [43] R. T. Zhang, X. L. Zhu, X. Y. Li, L. Liu, S. F. Zhang, W. T. Feng, D. L. Guo, Y. Gao, D. M. Zhao, J. G. Wang, and X. Ma, *Phys. Rev. A* **95**, 042702 (2017).
- [44] R. T. Zhang, J. W. Gao, Y. W. Zhang, D. L. Guo, Y. Gao, X. L. Zhu, J. W. Xu, D. M. Zhao, S. Yan, S. Xu, S. F. Zhang, Y. Wu, J. G. Wang, and X. Ma, *Phys. Rev. Res.* **5**, 023123 (2023).
- [45] H. Zhang, X. Fléchar, A. Cassimi, L. Adoui, F. Frémont, D. Lecler, G. Cremer, L. Guillaume, D. Lelievre, A. Lepoutre, and D. Hennecart, *Phys. Rev. A* **60**, 3694 (1999).
- [46] E. Y. Kamber, M. A. Abdallah, C. L. Cocke, and M. Stöckli, *Phys. Rev. A* **60**, 2907 (1999).
- [47] T. Cao, T. Meng, Y. Gao, S. F. Zhang, R. T. Zhang, S. Yan, X. L. Zhu, J. Wang, P. Ma, B. Ren, Z. H. Xia, D. L. Guo, C. J. Zhang, K. Z. Lin, S. Xu, B. Wei, and X. Ma, *The Astrophysical Journal Supplement Series* **266**, 20 (2023).
- [48] M. van der Poel, C. V. Nielsen, M.-A. Gearba, and N. Andersen, *Phys. Rev. Lett.* **87**, 123201 (2001).
- [49] M. van der Poel, C. V. Nielsen, M. Rybaltov, S. E. Nielsen, M. Machholm, and N. Andersen, *J. Phys. B: At. Mol. Opt. Phys.* **35**, 4491 (2002).
- [50] Q. Wang, X. Ma, X. L. Zhu, and S. F. Zhang, *J. Phys. B: At. Mol. Opt. Phys.* **45**, 025202 (2012).
- [51] H. Agueny, *Phys. Rev. A* **92**, 012702 (2015).
- [52] Md Abul Kalam Azad Siddiki, J. Mukherjee, K. Kumar, K. Tórkési, D. Misra, and H. Agueny, *Phys. Rev. Res.* **6**, 013108 (2024).
- [53] C. Cocke, L. Tunnell, W. Waggoner, J. Giese, S. Varghese, E. Kamber, and J. Pedersen, *Nucl. Instrum. Methods B* **24-25**, 97 (1987).
- [54] J. Edens, E. Kamber, K. Akgüngör, and S. Ferguson, *Nucl. Instrum. Methods B* **111**, 27 (1996).